Viscous and Elastic Fingering Instabilities in Foam

S. S. Park and D. J. Durian
Department of Physics, University of California, Los Angeles, California 90024-1547
(Received 4 November 1993)

We investigate pattern formation in the immiscible displacement of foam from a confining geometry. The dominant length scales with the driving pressure gradient as for a Newtonian fluid, but depends surprisingly on the ratio of plate separation to bubble diameter. The pattern morphology exhibits a transition from a jagged, presumably elastic, character to a smooth, viscous character as the shear strain rate rises far above the natural internal relaxation time scale of the foam. These features may result from the two-dimensional nature of the flows and the unusual rheology of foams.

PACS numbers: 47.20.−k, 47.54.+r, 82.70.Rr, 83.50.Nj

Pattern formation from two-phase flow instabilities has been intensely studied for the displacement of a viscous fluid from between parallel plates [1] or from a porous medium [2]. Such problems have obvious importance for resource recovery, and have gained fame as perhaps the most tractable type of fluid "chaos" where a complex dynamical structure evolves because of nonlinearity in a simple system. Recent work encompasses viscoelastic fluids [3,4] which have decreasing viscosity and increasing elasticity at higher strain rates, such as polymer solutions [5,6] or colloidal pastes [7], and provides insight on the fracture of solids [8]. Here we report on fingering and fracturelike phenomena in the immiscible displacement of a strikingly different non-Newtonian fluid: aqueous foam. In contrast to viscoelastic materials, foams have a static shear modulus, are purely viscous at high shear strain rates, and can exhibit plug flow [9]. Such rheology originates in the close packing of deformable gas bubbles, which typically compose more than 90% of the foam by volume, but is still in the early stages of quantitative understanding; for example, recent theories are beginning to incorporate polydispersity in the bubble size distribution, but are still limited to two-dimensional structures [10]. Experimentally, the difficulty in elucidating foam rheology lies both in characterizing foam microstructures and in creating rheometric flows [9,11]. The former issue is being attacked by the development of new multiple light scattering techniques [12], and the latter issue is circumvented here by the examination of flow instabilities where the formation of a pattern permits unambiguous characterization of imposed shear strain rates. Our experiments highlight the nature of foam rheology, reveal the important time and length scales for comparison with theory, and demonstrate consequences relevant for applications involving multiphase foam flows.

We use two radial Hele-Shaw cells made of $\frac{1}{4}$ in. plate glass with 25 and 50 cm edge lengths, respectively. The plate separation b is set to either 0.034, 0.056, 0.104, 0.206, or 0.262 cm. Foam samples are obtained from a commercial shaving cream whose structure and dynamics are reproducible and have been previously characterized both visually and by multiple light scattering [12]. It consists of nearly spherical hydrocarbon gas bubbles, average diameter 30 μm, dispersed in 7.5% soapy water; the liquid-vapor surface tension is $\sigma = 30$ ergs/cm^2. Circular samples of controlled radius R are ensured by flowing foam into a preassembled cell through its central hole; the plate separation is sufficiently great that samples appear homogeneous and white. The foam is displaced radially by N_2 blown into the same hole; constant driving pressures between 1 and 20 kPa above atmosphere are achieved by buffering the gas through a reservoir.

By contrast with usual viscous fingering [13], a thick wetting layer of foam is not left behind the advancing gas-foam interface. Instead, the foam flows as a plug; residue is left behind only at higher growth rates, and is never more than two or three bubble diameters thick. The sharp gas-foam interface is therefore easily detected with a charge-coupled device (CCD) camera and recorded by VCR for subsequent digitization. Pattern evolution for two sets of flow conditions is displayed in Fig. 1. Before addressing apparent differences in morphology, we consider the dominant length scales. For each pattern we measure the average finger width λ, which Fig. 1 reveals to be nearly independent of time. We also measure the mixing zone length L defined as the radial distance over which the gas-foam interface exists; the ratio L/λ quantifies the degree of branching.

The variation of finger width λ with flow conditions is summarized in Fig. 2. Three symbols distinguish flow cells and/or sample radii; for each we use five plate separations and approximately fifteen driving pressures for a total of 170 runs. The inset is for $b = 0.104$ cm, and demonstrates that the finger width obeys $\lambda \propto \sqrt{R/P}$ at constant plate separation when the driving pressure P and the sample radius R are independently varied. Identical behavior is found for the two smaller plate separations; for the larger two, however, the deviation from $\lambda \propto \sqrt{R/P}$ at low pressure gradients, marginally apparent in the inset, becomes marked.

The data collapse for cells of different edge lengths is further significant in implying that any plate flexing is unimportant. Nevertheless, we have measured the flexing at high pressures and find it can be as large as 0.2 ± 0.1

0031-9007/94/72(21)/3347(4)$06.00

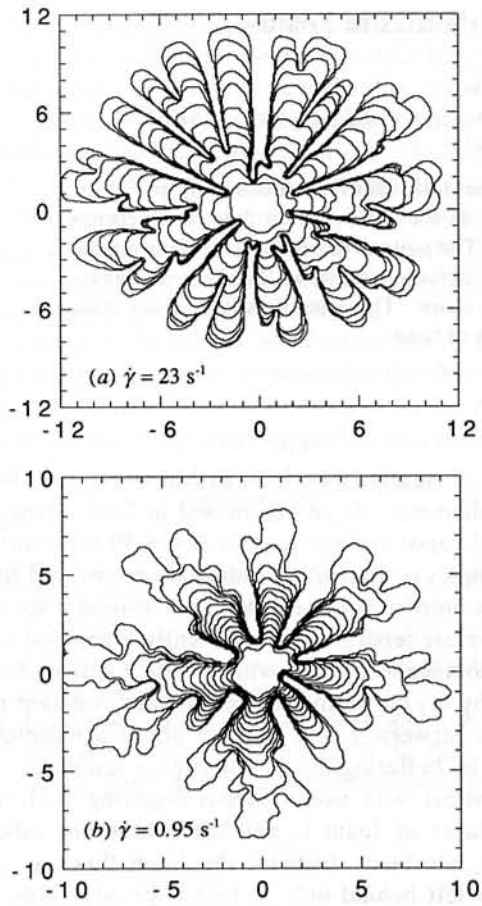

FIG. 1. Pattern formation in cm for foam displacement at high (a) and low (b) shear strain rates. For (a), the time interval between traces is $\Delta t = \frac{1}{60}$ s, the plate separation is $b = 0.104$ cm, the driving pressure is $P = 10$ kPa, and the sample radius is $R = 13.6$ cm. For (b), $\Delta t = 0.5$ s, $b = 0.034$ cm, $P = 6$ kPa, and $R = 13.0$ cm.

mm; this is a large fraction of the smallest gap measured, $b = 0.34$ mm.

The finger width behavior shown in the inset of Fig. 2 can be compared with the linear stability analysis of a flat interface advancing into a Newtonian fluid of viscosity μ. The fastest growing mode has predicted wavelength $\lambda = \pi b\sqrt{\sigma/\mu V}$ where the flow velocity, $V = (b^2/12\mu)\nabla P$, is set by viscous dissipation from the parabolic velocity profile between the plates [1]. For a radial Hele-Shaw experiment, crude estimation of the relevant pressure gradient from the driving pressure and sample radius, $\nabla P \cong P/R$, gives $\lambda\sqrt{P/\sigma R} \cong \pi\sqrt{12}$ independent of plate separation and viscosity. These arguments ignore the three-dimensional nature of viscous flows in neglecting the wetting layer and also in taking the pressure drop across the interface as σ/λ, rather than on the order of σ/b. We find that such three-dimensional effects are less crucial in our experiments, where the foam flows as a two dimensional plug. In particular, the main plot of Fig. 2 shows that $\lambda\sqrt{P/\sigma R}$, though not equal to $\pi\sqrt{12}$, extrapolates to

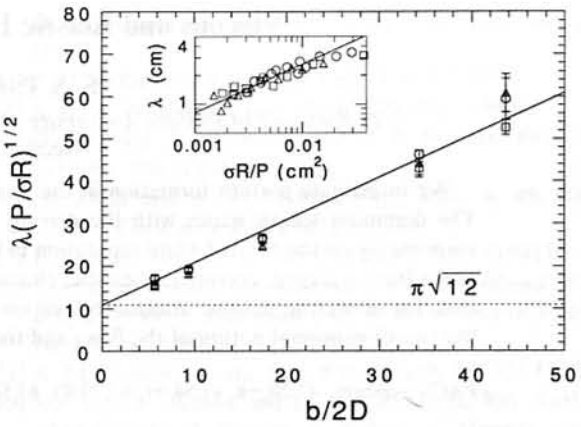

FIG. 2. Scaling of the finger width, λ, with flow conditions. The pressure gradient dependence is $\lambda \propto (P/R)^{-1/2}$ at constant plate separation, as shown for $b = 0.104$ cm in the inset. The proportionality constant increases with b divided by bubble diameter as shown in the main figure. Circles are for $R \cong 20$ cm; squares and triangles are for $R \cong 10$ cm but different sample cells.

this ideal value at $b = 0$. The full finger width scaling shown by the solid line in the main plot of Fig. 2 is

$$\lambda\sqrt{P/\sigma R} = \pi\sqrt{12} + b/2D\,, \qquad (1)$$

where D is the average bubble diameter in the foam. The empirical $b/2D$ term in Eq. (1) has no theoretical justification as yet, but it is reasonable that the bubble diameter sets the length scale for the plate separation below which the problem is essentially two dimensional.

Returning to the patterns of Fig. 1, note that they have comparable finger widths and degrees of branching, but are nevertheless qualitatively distinct. In Fig. 1(a), the fingers advance at roughly constant velocity, and the pattern closely resembles those found in ordinary viscous fluids [14,15]; we call such patterns type A. In Fig. 1(b), the fingers advance more slowly, but at an accelerating rate, and appear more jagged and less closely aligned with the radial direction; we call such new patterns type B. Another difference is that type A patterns develop by tip splitting, while type B patterns show evidence of side-branching as in the fracture of a solid [8]. Attempts to quantify the A-B distinction are still in progress; we note only that the fractal dimension is close to $\frac{7}{4}$ for both types and therefore does not suffice. Patterns are currently classified as type A or B based on perceived jaggedness and growth mode; to minimize bias, we viewed the videotapes in a random order without knowing the flow conditions. We also restrict attention to patterns satisfying $4 < L/\lambda < 9$ to avoid those which are underdeveloped or too highly branched and fast growing for confident A-B discrimination.

In order to correlate pattern morphology with foam rheology, we consider the typical shear strain rate $\dot{\gamma}$ imposed on the foam during pattern formation. Since the

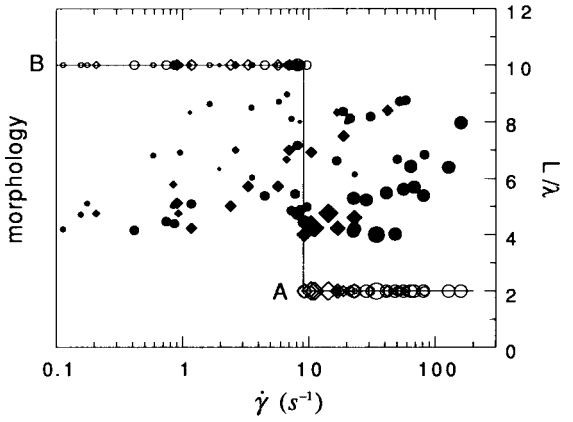

FIG. 3. Morphology (open/left scale) and degree of branching (solid/right scale) for patterns vs the shear strain rate in the foam during their formation. Note that for each open point plotted on the left scale, there is a solid point analog plotted on the right scale; also note that for given strain rate there are patterns with a range of branching degrees but which all have the same morphology. A transition between smooth, tip-splitting viscous fingering patterns (type *A*) and jagged, sidebranching patterns (type *B*) occurs at $\dot{\gamma}_c = 9\ s^{-1}$. Circles are for $R \cong 10$ cm; diamonds are for $R \cong 20$ cm; symbol size increases with plate separation.

flows are pluglike with velocity gradients primarily parallel to the plates, $\dot{\gamma}$ can be estimated as the ratio of finger velocity to finger width. Patterns of comparable $\dot{\gamma}$, but with degrees of branching varied in the range $4 < L/\lambda < 9$, are produced from different combinations of plate separation, sample radius, and driving pressure; all are found to have the same morphology type. This consistency test is demonstrated graphically in Fig. 3, where the morphology and degree of branching of each pattern is shown versus the shear strain rate during its formation. We conclude that pattern morphology is controlled simply by the shear strain rate in the foam.

The morphology transition apparent in Fig. 3 at $\dot{\gamma}_c = 9\ s^{-1}$ may be qualitatively understood from generic features of foam rheology. For large $\dot{\gamma}$ flows, the shear stress in foam is viscous in origin due to dissipation in the liquid films between sliding bubbles [9]; here, accordingly, we find type *A* viscous fingering patterns. For smaller $\dot{\gamma}$, where type *B* patterns are found, the shear stress is elastic in origin due to surface tension and the corresponding energy required to distort individual bubbles [9]. We therefore believe that elastic effects at low shear strain rates are responsible for the jaggedness and sidebranching of type *B* patterns, while viscous dissipation from bubble rearrangements in high shear strain rate flows gives rise to the classic viscous fingering patterns. This contrasts with fingering phenomena observed in conventional viscoelastic materials, where fracturelike behavior occurs at high strain rates and viscous behavior occurs at low strain rates [6,7]. Furthermore, foams are not simply the opposite of conventional viscoelastic materials because the two show quite different morphologies away from their viscous regimes. Another explanation of the morphology transition which cannot be discounted is that stick-slip motion at the moving contact line may contribute to the jaggedness of the patterns seen in foams; this seems unlikely, however, since the observed transition occurs as a function of strain rate rather than interface velocity.

It is interesting to compare the location of the morphology transition, at $\dot{\gamma}_c = 9\ s^{-1}$, with the known time scales in our foam. Aqueous foams are nonequilibrium systems which evolve with time by drainage, film rupture, or, as in our foam, by the diffusion of gas from smaller to larger bubbles. About 20 min is required for the bubble size distribution in fresh samples of our foam to noticeably coarsen [12]; this time scale is much longer than the duration of pattern formation and cannot be relevant. A faster time scale, however, arises as a consequence of coarsening. As the bubble size distribution changes infinitesimally, local strains develop since neighboring bubbles are packed so closely as to prevent continual adjustment to optimal arrangement. When such strains reach threshold, a sudden avalanchelike arrangement event is triggered in which many neighboring bubbles quickly hop around one another and relieve local elastic stresses. The average time interval τ_0 between rearrangement events at a given point in our foam is much longer than the duration of a typical event; diffusing-wave spectroscopy measurements give $\tau_0 = 8$ s in fresh samples [12]. Since a series of isolated rearrangement events could relieve stress from a macroscopically imposed strain, their natural rate of occurrence may be expected to separate elastic from viscous responses. However, this is not borne out since the shear strain rate at transition, $\dot{\gamma}_c = 9\ s^{-1}$, is 2 orders of magnitude faster than the rate τ_0^{-1} of rearrangement events. For foam to melt in response to applied shear strain, perhaps some larger scale collective motion is required, such as the percolation across the sample of shear-induced rearrangement events. Or, it may be relevant that the value of $\dot{\gamma}_c^{-1}$ is close to the measured duration of rearrangement events: At strain rates high in comparison with the event duration, the bubbles are in constant motion, and the foam therefore behaves viscously, since rearrangements are induced faster than bubbles can lock into close-packed configurations which can support stress elastically.

To conclude, the behavior of finger width and pattern morphology has been studied as a function of flow conditions, and can be related to foam rheology. Three relevant parameters are identified: the surface tension divided by the driving pressure gradient, the plate separation in comparison with the bubble diameter, and the shear strain rate in comparison with the foam's internal dynamics. It remains a theoretical challenge to quantitatively understand the length and time scales in the latter two. While resolution of these issues would illuminate

the relation of the microscopic structure and dynamics of a common and important form of matter to its macroscopic rheology, the difficulty is not unlike those encountered in granular flows and earthquake dynamics. For foam flows, nonlinearity arises from both the large distortion of bubbles and their sudden avalanchelike rearrangements. The nearly two-dimensional nature of plug flows, combined with the well-known behavior of the soap films at the microscopic level, may permit theoretical attacks not possible on other dynamical systems.

We thank J. V. Maher, S. M. Troian, and A. J. Liu for helpful conversations, and acknowledge the Donors of the Petroleum Research Fund, administered by the American Chemical Society, for partial support of this research.

[1] See, e.g., D. Bensimon *et al.*, Rev. Mod. Phys. **58**, 977 (1986); *Dynamics of Curved Fronts*, edited by P. Pelce (Academic Press, Boston, 1988); *Random Fluctuations and Pattern Growth*, edited by H. E. Stanley and N. Ostrosky (Kluwer, Boston, 1988).

[2] R. Lenormand and C. Zarcone, Phys. Rev. Lett. **54**, 2226 (1985); D. A. Weitz, J. P. Stokes, R. C. Ball, and A. P. Kushnick, Phys. Rev. Lett. **59**, 2967 (1989); J.-C. Bacri, D. Salin, and R. Woumeni, Phys. Rev. Lett. **67**, 2005 (1991).

[3] P. G. de Gennes, Europhys. Lett. **3**, 195 (1987).

[4] S. D. R. Wilson, J. Fluid Mech. **220**, 413 (1990).

[5] G. Daccord, J. Nittmann, and H. E. Stanley, Phys. Rev. Lett. **56**, 336 (1986).

[6] H. Zhao and J. V. Maher, Phys. Rev. A **45**, R8328 (1992); Phys. Rev. E **47**, 4278 (1993).

[7] E. Lemaire *et al.*, Phys. Rev. Lett. **67**, 2009 (1991).

[8] *Statistical Models for the Fracture of Disordered Media*, edited by H. J. Hermann and S. Roux (North-Holland, New York, 1990).

[9] A. M. Kraynik, Annu. Rev. Fluid Mech. **20**, 325 (1988).

[10] See, e.g., F. Bolton and D. Weaire, Phys. Rev. Lett. **65**, 3449 (1990); D. Weaire, F. Bolton, T. Herdtle, and H. Aref, Philos. Mag. Lett. **66**, 293 (1992); T. Okuzono, K. Kawasaki, and T. Nagai, J. Rheol. **37**, 571 (1993); D. C. Morse and T. A. Witten, Europhys. Lett. **22**, 549 (1993).

[11] J. P. Heller and M. S. Kuntamukkula, Ind. Eng. Chem. Res. **26**, 318 (1987).

[12] D. J. Durian, D. A. Weitz, and D. J. Pine, Science **252**, 686 (1991); Phys. Rev. A **44**, R7902 (1991).

[13] P. Tabeling, G. Zocchi, and A. Libchaber, J. Fluid Mech. **177**, 67 (1987).

[14] L. Patterson, J. Fluid Mech. **113**, 513 (1981).

[15] S. N. Rausseo, J. P. D. Barnes, and J. V. Maher, Phys. Rev. A **35**, 1245 (1987).